ARTICLE

ACS chemical biology

Influence of Charge on Cell Permeability and Tumor Imaging of GPR30-Targeted ^{111}In-Labeled Nonsteroidal Imaging Agents

Tapan K. Nayak[†,‡], Megan K. Dennis[†], Chinnasamy Ramesh[⊥], Ritwik Burai[⊥], Robert W. Atcher[‡,§,#], Larry A. Sklar[‡,§,∥], Jeffrey P. Norenberg[‡,§], Helen J. Hathaway[†,§], Jeffrey B. Arterburn[⊥,§], and Eric R. Prossnitz[†,§,*]

[†]Department of Cell Biology and Physiology, [‡]College of Pharmacy, [§]UNM Cancer Center, and [∥]Department of Pathology, University of New Mexico Health Science Center, Albuquerque, New Mexico 87131, [⊥]Department of Chemistry and Biochemistry, New Mexico State University, Las Cruces, New Mexico 88003, [#]Bioscience Division, Los Alamos National Laboratory, Los Alamos, New Mexico 87545

ABSTRACT Recent clinical studies implicate the role of G protein-coupled estrogen receptor, GPR30, in aggressive forms of breast, ovarian, and endometrial cancers. However, the functional role of GPR30 at cellular and molecular levels remains less clear and controversial, particularly its subcellular location. The primary objective of this study was to develop radiolabeled neutral and charged GPR30-targeted nonsteroidal analogues to understand the influence of ligand charge on cell binding, cellular permeability, and *in vivo* tumor imaging. Therefore, we developed a series of GPR30-targeted $^{111/113}$In(III)-labeled analogues using macrocyclic and acyclic polyamino-polycarboxylate chelate designs that would render either a net negative or neutral charge. *In vitro* biological evaluations were performed to determine the role of negatively charged analogues on receptor binding and activation using calcium mobilization and phosphoinositide 3-kinase assays. *In vivo* evaluations were performed on GPR30-expressing human endometrial Hec50 tumor-bearing mice to characterize the biodistribution and potential application of GPR30-targeted imaging agents for translational research. *In vitro* functional assays revealed an effect of charge, such that only the neutral analogue activated GPR30-mediated rapid signaling pathways. These observations are consistent with expectations for initial rates of membrane permeability and suggest an intracellular rather than the cell surface location of functional receptor. *In vivo* studies revealed receptor-mediated uptake of the radiotracer in target organs and tumors; however, further structural modifications will be required for the development of future generations of GPR30-targeted imaging agents with enhanced metabolic properties and decreased nonspecific localization to the intestines.

Estrogen plays an important role in a variety of normal physiological and pathological processes. Estrogen exerts many of its effects *via* the two known nuclear estrogen receptors (ERs), ERα and ERβ (*1*). In 2000, GPR30, an orphan seven transmembrane G protein-coupled receptor (GPCR), was shown to be involved in estrogen-mediated activation of ERK1/2 in cells lacking ERα but expressing GPR30, implicating a role for GPR30 in rapid estrogen-mediated cellular responses (*2*). In 2005, two studies reported estrogen binding to GPR30 and further characterized relationships between GPR30 expression and rapid estrogen-mediated signaling events (*3, 4*). Novel fluorescent estrogen derivatives (E2-Alexas) were used to examine the cellular and subcellular localization of GPR30 using confocal microscopy (*3*). The microscopy studies revealed that E2-Alexas detected ERα and ERβ in the nucleus of the cells, whereas GPR30 was predominantly located in the endoplasmic reticulum with no detectable signal at the plasma membrane. Most GPCRs are localized in the plasma membrane; therefore, to investigate this unexpected observation further, we developed a novel class of 17α-substituted small-molecule estrogen derivatives exhibiting differential cell permeability (*5*). This new class of estrogen derivatives revealed that positively charged cell-impermeable molecules did not activate rapid GPR30 or ER signaling, whereas the neutral cell-permeable molecules rapidly activated both ER and GPR30 in cell-based functional assays (*5*). These results confirmed the predominantly intracellular location of functional GPR30, as indicated by previous confocal microscopy studies (*3*). However, other studies have reported the presence of GPR30 on

*Corresponding author, eprossnitz@salud.unm.edu.

Received for review March 16, 2010 and accepted May 20, 2010.

Published online May 20, 2010

10.1021/cb1000636

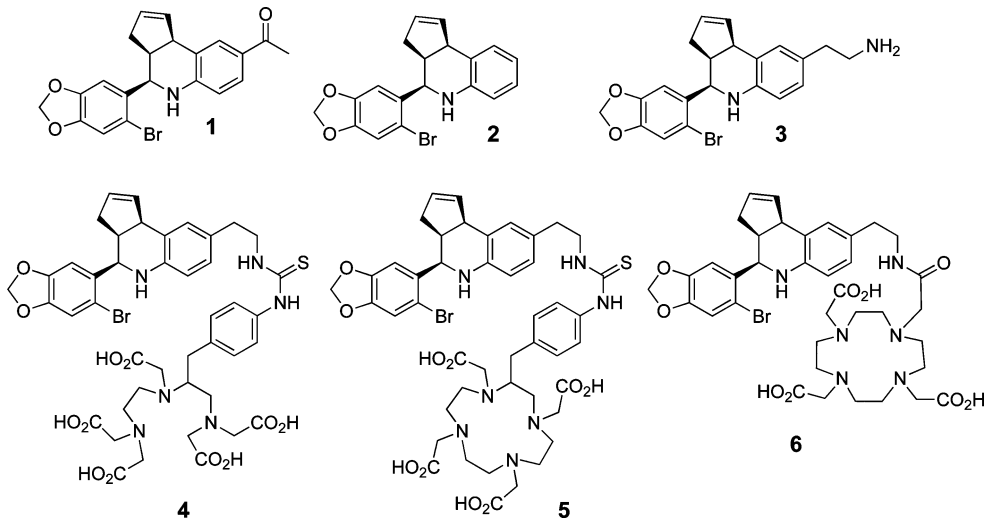

Figure 1. Chemical structures of parent and functionalized GPR30-targeted analogues: GPR30-agonist G-1 (1); GPR30-antagonist G15 (2); functionalized GPR30 derivative G-amine (3); GPR30-targeted analogue based on an acyclic polyamino-polycarboxylate DTPA chelate design, G-Bz-DTPA (4); and GPR30-targeted analogues based on macrocylic polyamino-polycarboxylate DOTA chelate designs, G-Bz-DOTA (5) and G-DOTA (6).

the cell surface, suggesting that a small fraction of total cellular receptor may be present at the cell membrane as a result of limited export and/or rapid constitutive internalization (*4, 6*). Nevertheless, it appears that estrogen must traverse the plasma membrane for functional activity of GPR30.

We have previously described a GPR30-selective agonist, G-1 (**1**), and recently a structurally related GPR30-selective antagonist, G15 (**2**) (Figure 1) (*7, 8*). Significant biological roles of GPR30 in physiological and pathological processes have been revealed using these GPR30-selective ligands (*8–12*). GPR30 knockout mice (in some cases in conjunction with GPR30-selective ligands) are also beginning to address the functions of GPR30 *in vivo* (*13, 14*). Recent clinical studies indicate that GPR30 is expressed in and associated with aggressive forms of breast, endometrial, and ovarian cancer that display low survival rates (*15–17*).

Estrogen has been a widely studied radiopharmaceutical target over the past 35 years. The most successful radiolabeled estrogen derivative, 16α-^{18}F-17β-estradiol (FES) is well characterized in patients with breast, uterine, ovarian and endometrial cancer (*18–21*). FES has been used clinically with promising results in imaging ER-expressing tumors and to evaluate responsiveness of tumors to anti-estrogen drugs (*18, 22, 23*). To study the *in vivo* distribution and role of GPR30, we have developed GPR30-selective radioiodinated derivatives (*24*). However, these radioiodinated derivatives were unsuitable for *in vivo* use because of rapid metabolism, high lipophilicity, and poor *in vivo* targeting characteristics.

ER-targeted imaging agents employing macrocyclic and acyclic polyamino-polycarboxylate chelates such as DOTA and DTPA have been previously reported (*25–28*). An aspartic acid-linked 4-hydroxy-tamoxifen-DTPA ligand demonstrated receptor specificity; however, the binding affinity was 10-fold lower than that of tamoxifen (*25*). Another DTPA-tamoxifen analogue with affinity similar to that of tamoxifen was evaluated for imaging ER-positive lesions (*27*). Biodistribution, autoradiography, and radionuclide imaging demonstrated *in vivo* receptor-specificity of the ^{111}In-labeled DTPA-tamoxifen conjugate, and tumors could be clearly visualized even after 48 h (*27*). In another report, estradiol was labeled with ^{177}Lu using *p*-SCN-DOTA as the chelating agent, and *in vitro* cell binding studies demonstrated receptor specificity (*26*). Despite the success of polyamino-polycarboxylate chelate designs for ER-targeting, a major concern is the possibility that a net charge can hinder receptor-binding kinetics resulting from limited cell permeability.

We have previously shown that a net positive charge can hinder cell permeability of a derivatized estrogen molecule in short-term experiments (seconds to minutes), although the ligand retains receptor specificity and can activate cell signaling over prolonged time periods (hours) (*5*). The goals in the current study were to understand the influence of charge of the chelate ligand on cell binding, permeability, and tumor imaging. Therefore, we conjugated the tetrahydro-3*H*-cyclopenta-[*c*]quinoline amine (**3**), based on the chemical scaffold of the novel GPR30-selective ligands G-1 and G15, with *p*-SCN-DTPA, *p*-SCN-DOTA, and DOTA to provide the corresponding aminocarboxylate chelate ligands (**4**–**6**). These chelates were labeled with $^{111/113}$In and evalu-

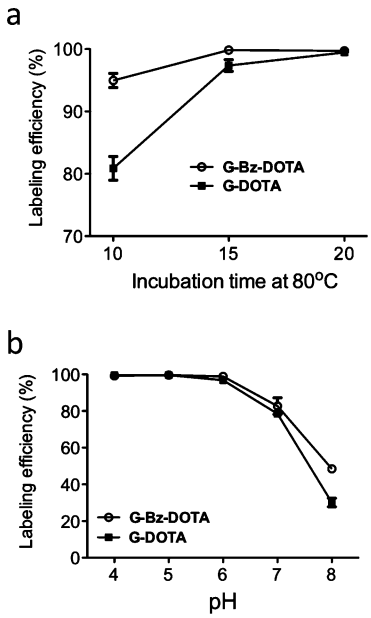

Figure 2. Labeling efficiency of G-DOTA and G-Bz-DOTA. Influence of (a) incubation time and (b) pH on ^{111}In labeling efficiency of G-DOTA and G-Bz-DOTA.

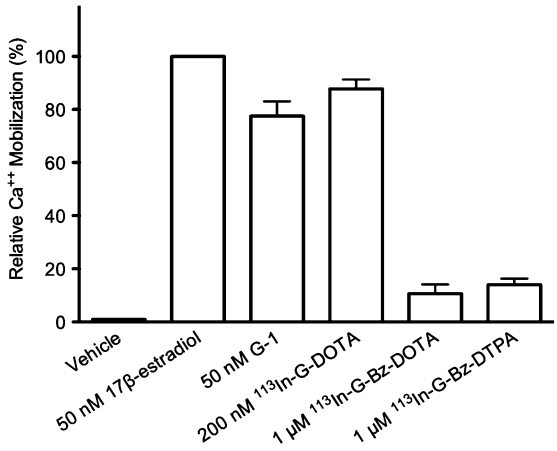

Figure 3. Mobilization of intracellular calcium by ^{113}In-labeled derivatives. The effects of ^{113}In-labeled derivatives and known GPR30 agonists were evaluated in indo1-AM-loaded SKBr3 cells. Calcium mobilized by 50 nM 17β-estradiol at 3 min post stimulation was defined as 100% and the effects of other ligands compared to this response. All data represent the mean ± SEM from three independent experiments.

ated using cell-based ligand-binding and functional biological assays to characterize the role of anionic charged chelate complexes [^{111}In-G-Bz-DTPA]$^{2-}$ and [^{111}In-G-Bz-DOTA]$^{-}$ on receptor binding and activation in comparison with a neutral complex [^{111}In-G-DOTA]. We then investigated the use of ^{111}In-labeled GPR30-targeted analogues to detect GPR30 *in vivo* using radioisotope-imaging modalities. In this report, we describe radiochemistry experiments (examining the role of pH and incubation time on labeling efficiency), cell permeability, and GPR30 functional assays (to assess ligand-chelate activity), as well as *in vivo* biodistribution and imaging studies on GPR30-expressing human endometrial cancer-bearing female mice.

RESULTS AND DISCUSSION

In this study, we developed neutral and negatively charged GPR30-selective indium-labeled polyaminopolycarboxylate compounds for *in vivo* targeting of GPR30 and potential use as cancer diagnostic and therapeutic agents. We designed this series of aminocarboxylate chelates based on the tetrahydro-3*H*-cyclopenta[*c*]quinoline scaffold that we have previously demonstrated binds to GPR30 with high selectively. The removal of the ethanone functional group at the C8 position of G-1, yielding G15, changes the GPR30-mediated activity from agonism to antagonism, while maintaining strong relative binding affinity for GPR30 (*8*). Therefore, we anticipated that introduction of an alkylamine linkage at this C8 position would provide a derivative suitable for conjugation with amine-reactive chelates derivatives such as DOTA-NHS, *p*-SCN-Bz-DOTA, and *p*-SCN-Bz-DTPA to provide the desired GPR30-targeted aminocarboxylate chelates.

Synthetic Chemistry. The pendant aminoethyl derivative (G-amine, **3**) was prepared in 95% yield from the $Sc(OTf)_3$-catalyzed Povarov cyclization of 6-bromopiperonal, cyclopentadiene, and the ^{t}Boc-protected aminophenethylamine in acetonitrile, followed by deprotection with TFA/CH_2Cl_2 as previously described (*8*) and shown schematically in Supplementary Figure 1. The G-amine derivative was then coupled with the activated phenylisothiocyanate groups attached to the alkyl backbone of the aminocarboxylate chelates *p*-SCN-Bz-DTPA and *p*-SCN-Bz-DOTA to provide the thiourea-linked derivatives displaying free penta- and tetra-acetic acid groups, respectively (**4** and **5**) (Supplementary Figure 2). These derivatives were isolated by precipitation with ethanol and filtration, followed by water washes to provide the pure solid derivatives. The mono-*N*-hydroxysuccinimide ester of DOTA was coupled

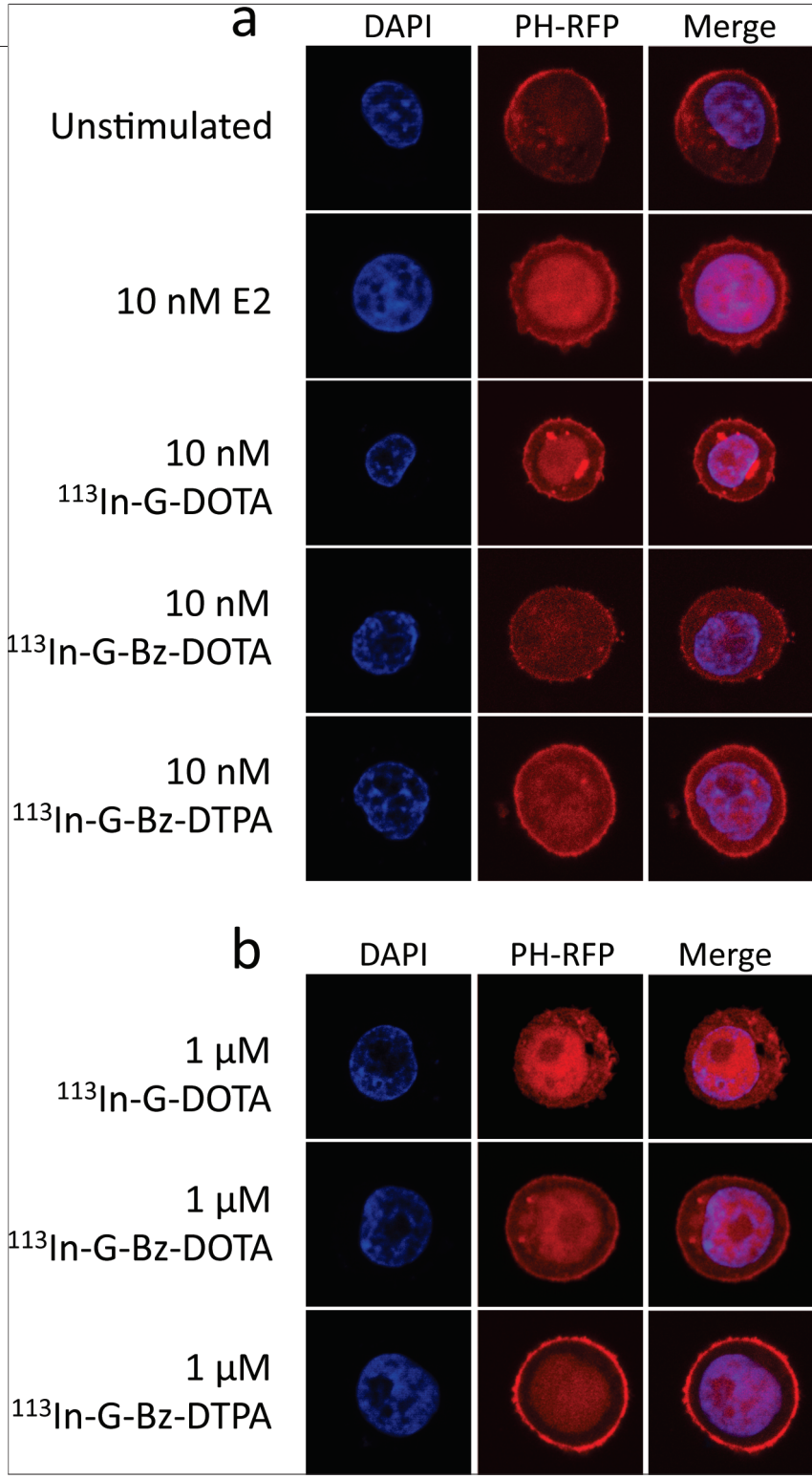

Figure 4. GPR30-mediated activation of PI3K by ^{113}In-labeled derivatives. The activity of ^{113}In-labeled derivatives was evaluated using SKBr3 cells transfected with the Akt-PH-mRFP1 reporter. 17β-Estradiol, ^{113}In-G-DOTA, ^{113}In-G-Bz-DOTA, and ^{113}In-G-Bz-DTPA were used at 10 nM (a) or 1 μM (b). Data are representative of three independent experiments.

with the G-amine derivative in dry DMF to provide the triacetic acid G-DOTA derivative (**6**) (Supplementary Figure 2). The connecting linkage of this G-DOTA chelate lacks the hydrophobic phenyl group that is present in the other derivatives, and therefore exhibited increased water solubility. The G-DOTA derivative was purified by reverse phase chromatography using a C18 column eluted with methanol/water (60:40).

Radiochemistry. After incubation at RT for 60 min, the labeling efficiency and radiochemical purity for ^{111}In-labeled G-Bz-DTPA were >99% and 95%, respectively, as determined by ITLC and HPLC (Supplementary Figure 3). Over 99% incorporation yield was obtained for ^{111}In-labeled G-Bz-DOTA and G-DOTA, when the reaction mixture was heated at 80 °C for 20 min at pH 4.5. The radiochemical purities as assessed by HPLC of ^{111}In-labeled G-DOTA (Supplementary Figure 3) and ^{111}In-labeled G-Bz-DOTA (Supplementary Figure 3) were over 95%. The HPLC analysis revealed the presence of two predominant isomeric complexes of the ^{111}In-labeled G-DOTA and ^{111}In-labeled G-Bz-DOTA compounds as seen in the representative chromatograms, while a single DTPA construct was observed under the reverse-phase chromatographic conditions used. The specific activity ranged from 35−60 MBq nmol^{-1} for all the derivatives. However, when the labeling reaction was performed at 100 °C for the DOTA derivatives, a degradation product was obtained, decreasing the radiochemical purity to as low as 70%. Very low incorporation yields for the DOTA derivatives were obtained when the reaction was carried out at 60 °C with an incubation time of 20 min.

Stability and Solubility. The ^{111}In-labeled G-DOTA, G-Bz-DOTA, and G-Bz-DTPA derivatives exhibited good stability (over 90%) after incubation at 37 °C for up to 4 days in PBS (pH 7.4) or mouse plasma. The ^{111}In-labeled G-Bz-DTPA would be expected to form a monomeric dianionic (2−) charged complex with In(III) at physiological conditions and exhibited a correspondingly low log $P_{(o/w)}$ value of

1.5 ± 0.1. The macrocyclic DOTA derivatives were significantly more lipophilic than the acyclic DTPA derivative, such that the neutral complex G-DOTA exhibited a log $P_{(o/w)}$ value of 4.8 ± 0.3, whereas the monoanionic benzyl-thiourea linked complex G-Bz-DOTA exhibited an increased log $P_{(o/w)}$ value of 5.2 ± 0.3.

Role of Incubation Time and pH on Labeling Efficiency. To study the role of incubation time on incorporation yield and labeling efficiency, G-DOTA and G-Bz-DOTA were incubated with $^{111}InCl_3$ at 80 °C and pH 5. The labeling kinetics were more rapid for G-Bz-DOTA than for G-DOTA (Figure 2, panel a). After 10 min of incubation, over 94% of the ^{111}In was incorporated into G-Bz-DOTA as compared to 80% for G-DOTA. The reduced rate of coordination to form the ^{111}In-G-DOTA complex compared with the ^{111}In-G-Bz-DOTA species may result from increased steric contraints and limited conformational flexibility associated with the direct carboxamide linkage between the DOTA nitrogen and the GPR30-targeting quinoline derivative. Monoclonal antibodies have been successfully radiolabeled with ^{111}In at pH 7 and higher with incorporation yields of over 90% (*29, 30*). However, for hydrophobic small molecules, G-DOTA and G-Bz-DOTA, the best incorporation yields were achieved between pH 4 and 6, which may be related to the isoelectric point of the agent, offering better solution stabilization and thermodynamics at pH 4−6 (*29*).

To examine the role of pH, G-DOTA and G-Bz-DOTA were incubated with ^{111}In at 80 °C for 20 min from pH 4 to 8. Optimum radiolabeling (over 95% incorporation) was achieved between pH 4 and 6 (Figure 2, panel b). At pH 8, incorporation yields were as low as 25%. At pH values >5, G-DOTA labeling was more dependent on pH than G-Bz-DOTA, presumably because of differences in pK_a, deprotonation rates, and electrostatic repulsion between these two derivatives (*31*).

***In Vitro* Cellular Activity.** GPR30 activation by either estrogen or G-1 has been shown to initiate a number of signal transduction cascades in cells. These include intracellular calcium mobilization and activation of a number of kinases, such as epidermal growth factor receptor (EGFR), mitogen-activated protein kinase (MAPK), and phosphatidylinositol 3-kinase (PI3K). In order to investigate the functional properties of the chelate series on endogenous GPR30 expressing cells, the corresponding stable isotope ^{113}In-labeled derivatives were assessed for their ability to mobilize intracellular calcium in GPR30-positive, ERα/β-negative SKBr3 cells. The ^{113}In-labeled derivatives carrying a net negative charge, ^{113}In-G-Bz-DOTA and ^{113}In-G-Bz-DTPA, were unable to significantly mobilize calcium in these cells within a time frame (3 min) consistent with rapid signaling, whereas the neutral ^{113}In-G-DOTA compound was effective in a time frame comparable to G-1 (maximal response in 15−20 s) (Figure 3). This result suggests that, even applied at a higher concentration than their neutral counterparts, the net negative charge associated with these compounds prevents their rapid entry into the cell and thus their rapid signaling *via* GPR30.

Additionally, the ^{113}In-labeled derivatives were used to assess PI3K activation utilizing an assay employing the PIP3-binding pleckstrin homology (PH) domain of AKT fused to mRFP (PH-RFP) to localize PIP3 production and accumulation in SKBr3 cells. Consistent with our findings in the calcium mobilization assay, stimulation of cells with ^{113}In-G-DOTA for 15 min resulted in the accumulation of the PH-RFP reporter in the nucleus, as has been observed for estrogen and G-1, indicative of GPR30-medated PI3K activation (Figure 4, panel a). Interestingly, the ^{113}In derivatives with net negative charges, ^{113}In-G-Bz-DOTA and ^{113}In-G-Bz-DTPA, were able to elicit a weak PI3K activation when administered to cells at higher doses (1 μM, Figure 4, panel b), but no PI3K activation was detected when cells were stimulated with low doses (10 nM) of these compounds. This result is consistent with our previous finding that charged compounds at high concentrations can activate PI3K *via* GPR30 when the cells are stimulated for longer times than in the calcium mobilization assay (3 min *vs* 15 min) (*5*). This may be due to either the slow entry of a low concentration of compound into the cytoplasm, where it can stimulate GPR30, or a small fraction of GPR30 present at the cell surface at some time during cell stimulation, although the latter is less likely because of the lack of calcium mobilization in these same cells over a 3 min time interval.

Radioligand binding assays using intact GPR30-expressing, ERα/β-negative Hec50 cells show that the ^{113}In-G-DOTA compound binds to GPR30 with an IC_{50} of 33.9 ± 2.4 nM. To evaluate the possible nonselective binding of ^{113}In-labeled derivatives to the classical estrogen receptor ERα, binding assays using ERα-transfected COS7 cells were performed. No detectable binding of any of the three ^{113}In-labeled derivatives to ERα was ob-

TABLE 1. Time-dependent biodistribution of the ^{111}In-G-DOTA derivative in selected organs of ovariectomized female athymic (NCr) *nu/nu* mice bearing GPR30-expressing human endometrial Hec50 tumors

Organs	0.5 h PI	1 h PI	2 h PI	2 h PI (block, 5 μg G-1)	4 h PI
Heart	5.87 ± 0.55[a]	1.46 ± 0.19	0.25 ± 0.04	0.19 ± 0.03	0.17 ± 0.02
Blood	3.94 ± 0.54	2.22 ± 0.34	1.21 ± 0.63	1.11 ± 0.17	0.23 ± 0.02
Lungs	4.98 ± 0.84	2.50 ± 0.44	0.80 ± 0.11	1.00 ± 0.23	0.48 ± 0.10
Liver	14.28 ± 1.50	12.04 ± 1.43	3.87 ± 0.41	4.98 ± 0.71	3.04 ± 0.73
Spleen	0.76 ± 0.06	1.04 ± 0.25	0.26 ± 0.07	0.91 ± 0.71	0.36 ± 0.10
Large intestine	1.29 ± 0.28	8.32 ± 1.03	15.27 ± 4.78	20.12 ± 3.19	8.48 ± 0.67
Small intestine	11.13 ± 0.84	19.43 ± 5.22	6.12 ± 3.96	2.32 ± 0.76	1.25 ± 0.11
Stomach	6.80 ± 0.99	5.05 ± 1.75	0.61 ± 0.18	0.61 ± 0.35	0.30 ± 0.08
Kidneys	2.55 ± 0.30	3.95 ± 0.43	1.62 ± 0.53	1.00 ± 0.16	1.74 ± 0.46
Adrenals	7.11 ± 0.51	5.02 ± 0.86	1.33 ± 0.08	0.55 ± 0.14	0.57 ± 0.08
Bone	1.32 ± 0.21	0.85 ± 0.39	0.17 ± 0.05	0.21 ± 0.08	0.12 ± 0.02
Muscle	0.69 ± 0.10	0.43 ± 0.11	0.13 ± 0.06	0.15 ± 0.03	0.08 ± 0.02
Uterus	1.46 ± 0.23	0.73 ± 0.09	0.69 ± 0.08	0.31 ± 0.06	0.66 ± 0.03
Mammary	1.16 ± 0.32	0.72 ± 0.24	0.44 ± 0.03	0.16 ± 0.02	0.50 ± 0.07
Pituitary	0.88 ± 0.06	0.60 ± 0.05	0.04 ± 0.03	0.15 ± 0.10	0.01 ± 0.00
Brain	0.33 ± 0.01	0.16 ± 0.08	0.06 ± 0.01	0.11 ± 0.06	0.05 ± 0.02
Urinary bladder	4.13 ± 0.39	1.50 ± 0.21	0.15 ± 0.05	0.50 ± 0.16	0.36 ± 0.16
Hec50 tumor	3.81 ± 0.18	1.58 ± 0.41	0.60 ± 0.03	0.44 ± 0.04	0.48 ± 0.02

[a]Uptake values are expressed as % ID g^{-1}. Data represent the mean value ± SEM from at least 3 determinations.

served (data not shown), indicating that the In-labeled derivatives are highly selective for GPR30.

Biodistribution in Hec50 Tumor-Bearing Animals. On the basis of the *in vitro* analysis, biodistribution was performed in Hec50 endometrial tumor-bearing animals by injecting 1.8 MBq of ^{111}In-G-DOTA in the tail vein of conscious mice. ^{111}In-G-DOTA demonstrated moderate tumor/blood and tumor/muscle ratios and rapid clearance. The tumor/blood ratio of 0.71 at 1 h PI increased to 2.08 at 4 h PI; similarly, the tumor/muscle ratio of 3.55 at 1 h PI increased to 6.00 at 4 h PI. The liver and the intestines exhibited the highest uptakes values (Table 1), although the uptake values in liver rapidly decreased over time (Figure 5, panel a). As a result of the hepatobiliary excretion, an opposite trend was observed in the intestines where the values increased over time (Figure 5, panel a). The observed pharmacokinetic trend in the liver, gall bladder, kidney, urinary bladder, and the intestines suggests hepatobiliary and urinary excretion and possible metabolism. Hydrophilic radiometabolites were observed in chromatograms of the collected urine samples (Supplementary Figure 4). Over 60% of the injected dose was excreted *via* the urinary and hepatobillary systems within 4 h PI, and the calculated half-life ($t_{1/2}$) was 2.9 h. At 0.5 and 1 h PI, high uptake was observed in nonspecific target organs such as stomach, bone and lungs; however, these values decreased over time (Table 1 and Figure 5, panel a). A similar trend was observed in the tumors, where uptake decreased from 3.81% to 0.48% ID g^{-1} between 0.5 and 4 h PI. Receptor-mediated uptake, determined by co-injection with excess unlabeled G-1, was observed in adrenal glands in addition to the uterus, mammary tissue, and the Hec50 tumor (Figure 5, panel b). The uptake values of the radiotracer in the uterus, mammary glands, tumor, and adrenal glands were significant when compared to the uptake values in the presence of excess unlabeled G-1.

Imaging Studies. Imaging studies were carried out after injecting 12.9 MBq ^{111}In-G-DOTA *via* the tail vein of Hec50 tumor bearing mice. Whole body 60 s/projection imaging studies were carried out under 1.5−1.7%

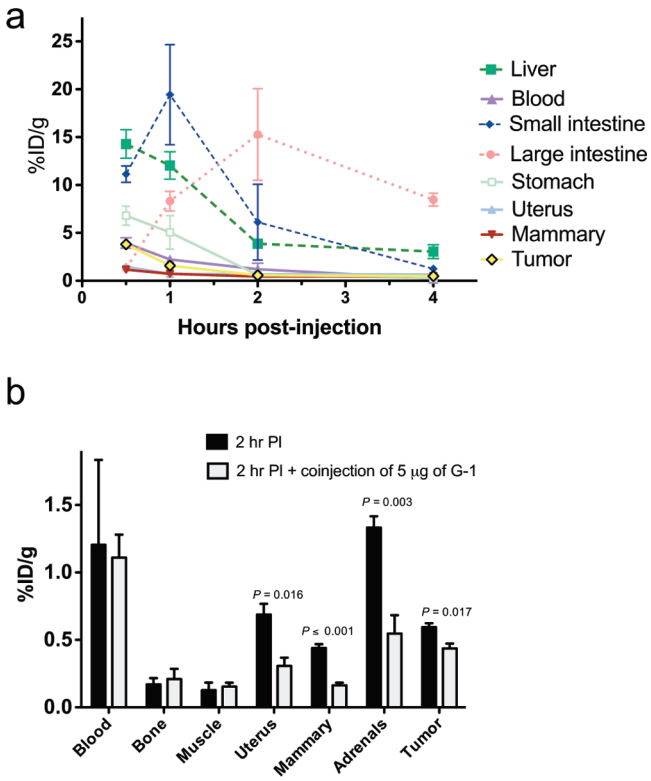

Figure 5. Biodistribution of ^{111}In-labeled G-DOTA. a) Time−activity curve and b) *in vivo* GPR30-specificity of ^{111}In-labeled G-DOTA in selected organs of ovariectomized female athymic (NCr) *nu/nu* mice bearing GPR30-expressing human endometrial Hec50 tumors. All uptake values are expressed as % ID g^{-1}. Data represent the mean value ± SEM from at least 3 determinations.

isoflurane using a temperature controlled bed (36−38 °C). Imaging studies revealed very high consistent activity in the intestines (Suppl. Figure 5a). Upon image quantification, the liver uptake decreased from 14.48% ID (1 h PI) to 3.13% ID (4 h PI); whereas the intestine uptake increased from 64.91% ID (1 h PI) to 83.88% ID (4 h PI). Tumors were visualized at 1 h PI; however, the nonspecific activity was very high, particularly in the bladder and the intestine (Suppl. Figure 5a). Nevertheless, activity in shoulder tumors (Suppl. Figure 5b) and flank tumors (Suppl. Figure 5c) was clearly visualized in transverse slices. At the same image threshold, the tumors were better visualized when the bladder was cropped from the image (Suppl. Figure 5d). Without decreasing the image threshold, shoulder tumors were clearly visualized on 200 s/projection focused studies (Figure 6), demonstrating the uptake of the radiotracer in the tumor. It is often desirable for a tracer to rapidly wash out from the nontarget organs and retain activity in the target organs for better target/background ratios. Although ^{111}In G-DOTA was rapidly washed out from nontarget organs, the activity was not retained in the target organs. Metabolism of the imaging agent that results in cleavage of the linkage, producing a metabolite that is excreted by an active transport pathway or otherwise significantly decreases GPR30 binding affinity, may be implicated. On the basis of these results,^{111}In G-DOTA does not represent an ideal imaging agent. Nevertheless, valuable information was obtained from the animal studies of these first

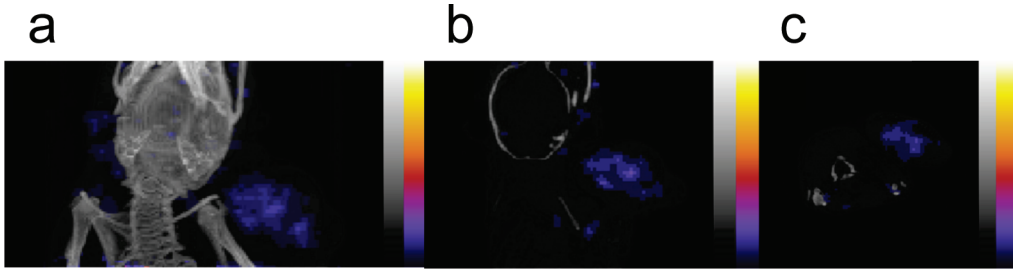

Figure 6. *In vivo* imaging of ^{111}In-labeled G-DOTA. Focused SPECT/CT 1 h PI images of ^{111}In-labeled G-DOTA in female in selected organs of ovariectomized female athymic (NCr) *nu/nu* mice bearing GPR30-expressing human endometrial Hec50 tumors. a) Maximum intensity projection, b) coronal slice of the tumor xenograft implanted on the shoulder, and c) transverse slice of the tumor xenograft.

generation G-polyamino-polycarboxylate acyclic and macrocyclic derivatives. Subsequent development should address structural modifications that increase the uptake in target tissues, maximize residence time, and decrease metabolism and nontarget organ uptake.

Conclusion. In this work, we have successfully synthesized and evaluated the first generation of nonsteroidal ^{111}In-labeled GPR30-targeted analogues for cancer imaging. The ^{113}In-labeled analogues demonstrated the intracellular functionality of GPR30 in whole-cell-based assays. The neutral ^{113}In-G-DOTA complex stimulated calcium mobilization consistent with rapid signaling *via* GPR30, whereas both anionic charged species failed to elicit a response. Analogous results were obtained using PI3-kinase activation assays, although the charged species [^{113}In-G-Bz-DOTA]$^{-}$ and [^{113}In-G-Bz-DTPA]$^{2-}$ could elicit weak responses at very high doses (1 μM). These results are consistent with previous findings and expectations for reduced membrane permeability of the charged species. The GPR30 binding affinity IC_{50} of 33.9 ± 2.4 nM of the neutral ^{113}In-G-DOTA complex was comparable to the similar small molecules G-1 (~11 nM) and G15 (~20 nM) from which the targeting agent was derived, and indicates that the presence of the neutral DOTA chelate structure at the C8 position does not significantly compromise receptor binding interactions. The radiochemistry experiments demonstrated efficient metal incorporation in the acyclic and macrocyclic polyaminocarboxylate chelate derivatives conjugated to a small, hydrophobic targeting agent. The biodistribution and imaging studies with ^{111}In-G-DOTA revealed moderate tumor/blood and tumor/muscle ratios, although unfavorable *in vivo* targeting characteristics and rapid clearance from the tumor were observed with this agent. Our results suggest hepatobiliary and urinary excretion and formation of polar metabolites were problematic. These studies provide a foundation for the further development of GPR30 targeted imaging agents.

METHODS

Details of chemical synthesis, purification and characterization are provided in Supporting Information.

Cell Culture. ERα/β-negative and GPR30-expressing human endometrial carcinoma Hec50 cells, ERα/β-negative and GPR30-expressing human breast carcinoma SKBr3, and ERα/β and GPR30-negative monkey kidney Cos-7 cells were cultured in DMEM tissue media (Hec50, Cos7) or RPMI-1640 tissue media (SKBr3) with fetal bovine serum (10%) and 100 units mL^{-1} penicillin and 100 μg mL^{-1} streptomycin. Cells were grown as a monolayer at 37 °C, in a humidified atmosphere of 5% CO_2 and 95% air. Lipofectamine2000 was used according to manufacturer's directions for all transfections.

Intracellular Calcium Mobilization. SKBr3 cells (1×10^7 mL^{-1}) were incubated in HBSS containing 3 μM Indo1 a.m. (Invitrogen) and 0.05% pluronic acid F-127 for 1 h at RT. Cells were then washed twice with HBSS, incubated at RT for 20 min, washed again with HBSS, resuspended in HBSS at a density of 10^8 cells mL^{-1}, and kept on ice until assay, performed at a density of 2×10^6 cells mL^{-1}. Ca^{2+} mobilization was determined ratiometrically using λ_{ex} 340 nm and λ_{em} 400/490 nm at 37 °C in a spectrofluorometer (QM-2000-2, Photon Technology International) equipped with a magnetic stirrer.

PI3K Activation. The PIP3 binding domain of Akt fused to mRFP1 (PH-RFP) was used to localize cellular PIP3. SKBr3 cells (transfected with PH-RFP) were plated on coverslips and serum starved for 24 h followed by stimulation with ligands as indicated. The cells were fixed with 2% PFA in PBS, washed, mounted in Vectashield containing DAPI (Vector Laboratories), and analyzed by confocal microscopy using a Zeiss LSM510 confocal fluorescence microscope.

Receptor-Binding Studies. To evaluate ligand binding to GPR30 expressed in Hec50 cells, competition binding was performed on selected ^{113}In-labeled GPR30-targeted derivative with a radioiodinated GPR30-targeted analogue (*8*). Hec50 cells (50−60% confluent) were washed twice with PBS solution, and the medium was replaced with phenol-red-free medium containing 10% charcoal-stripped fetal bovine serum and incubated overnight. Cells were washed three times with PBS and trypsinized. Approximately 75,000 cells per plate were plated in 24-well plates and incubated overnight in phenol-red-free, charcoal-stripped, serum-containing medium. On the day of the experiment, the plated cells were washed twice with PBS, and increasing doses of ^{113}In-labeled derivatives were added and incubated for 30 min. After the 30 min incubation period, ^{125}I-labeled GPR30-targeted analogue was added to each well and incubated for 1 h at 37 °C. Cells were washed three times with PBS to remove nonspecifically bound ^{125}I derivative. To extract the cells, ethanol was added to each well and incubated at 37 °C for 5 min. The radioactivity associated with the collected extract was then counted using a Wallac Wizard 1480 automatic gamma counter. To determine nonspecific binding, the cells were incubated with 10 μM G-1. The IC_{50} values were determined using in-built nonlinear regression analysis in GraphPad Prism version 5 software (San Diego, CA).

Binding assays for ERα were performed as previously described (*3*). Briefly, Cos7 cells were transiently transfected with ERα-GFP. Following serum starvation for 24 h, cells (~5×10^4) were incubated with ^{113}In-labeled derivatives for 10 min in a final volume of 10 μL prior to addition of 10 μL of 20 nM E2-Alexa633 in saponin-based permeabilization buffer. After 5 min at RT, cells were washed once with 1 mL of PBS/2% BSA, resuspended in 200 μL, and analyzed on a FACS Calibur flow cytometer (BD Biosciences).

Animal and Tumor Models. The human endometrial carcinoma Hec50 tumor model was developed by injecting 3−4 million Hec50 cells subcutaneously in 8-week-old female ovariectomized athymic (NCr) *nu/nu* mice (Harlan Inc., Indianapolis, IN).

After 4−6 weeks, tumors ranging from 0.5−0.7 cm in diameter were observed.

Biodistribution and SPECT/CT Imaging Studies. Conscious Hec50 tumor-bearing mice were injected intravenously (tail vein) with selected ^{111}In-labeled derivatives. To determine GPR30-receptor specificity, 5 μg of G-1 was premixed with the radiotracer and the two compounds were co-injected intravenously. At the desired time points, the animals were sacrificed by CO_2 inhalation. Urine and blood samples were collected for metabolism studies. After sacrificing the animals, organs were carefully removed and isolated to determine the biodistribution characteristics of the tracer. The organ samples were weighed, and the corresponding radioactivity was measured using an automated gamma counter after verifying the counting efficiency with standards. The percent-injected dose per gram of tissue (%ID g^{-1}) was calculated by comparison with standards representing the injected dose per animal.

NanoSPECT/CT Imaging studies were performed using a multipinhole NanoSPECT/CT small animal imager (Bioscan Inc., Washington, DC). Whole body imaging studies were carried out using 1.5−1.7% isofluorane on a temperature-controlled bed. All animal experiments were conducted in compliance with the guidelines and approved protocols established by the UNM Institutional Animal Care and Use Committee.

Statistical Analysis. All numerical data were expressed as the mean of the values ± the standard error of mean (SEM). GraphPad Prism version 5 (San Diego, CA) was used for statistical analysis, and a P of <0.05 was considered statistically significant.

Acknowledgment: This work was supported by NIH grants R01 CA127731 (JBA, ERP), CA118743 (ERP), and MH074425 (LAS) and MH084690 (LAS); the University of New Mexico Cancer Center (NIH P30 CA118100); the New Mexico Cowboys for Cancer Research Foundation (JBA); Oxnard Foundation (ERP); and the Stranahan Foundation (ERP). SPECT/CT images were generated in the Keck-UNM Small Animal Imaging resource established with funding from the W. M. Keck Foundation (LAS/ERP). Fluorescence microscopy images were generated in the University of New Mexico Cancer Center Fluorescence Microscopy Facility supported as at http://hsc.unm.edu/crtc/microscopy/Facility.html.

The authors declare no conflicts of interest.

Supporting Information Available: This material is available free of charge *via* the Internet at http://pubs.acs.org.

REFERENCES

1. Nilsson, S., Makela, S., Treuter, E., Tujague, M., Thomsen, J., Andersson, G., Enmark, E., Pettersson, K., Warner, M., and Gustafsson, J. A. (2001) Mechanisms of estrogen action, *Physiol. Rev. 81*, 1535–1565.
2. Filardo, E. J., Quinn, J. A., Bland, K. I., and Frackelton, A. R., Jr. (2000) Estrogen-induced activation of Erk-1 and Erk-2 requires the G protein-coupled receptor homolog, GPR30, and occurs *via* transactivation of the epidermal growth factor receptor through release of HB-EGF, *Mol. Endocrinol. 14*, 1649–1660.
3. Revankar, C. M., Cimino, D. F., Sklar, L. A., Arterburn, J. B., and Prossnitz, E. R. (2005) A transmembrane intracellular estrogen receptor mediates rapid cell signaling, *Science 307*, 1625–1630.
4. Thomas, P., Pang, Y., Filardo, E. J., and Dong, J. (2005) Identity of an estrogen membrane receptor coupled to a G protein in human breast cancer cells, *Endocrinology 146*, 624–632.
5. Revankar, C. M., Mitchell, H. D., Field, A. S., Burai, R., Corona, C., Ramesh, C., Sklar, L. A., Arterburn, J. B., and Prossnitz, E. R. (2007) Synthetic estrogen derivatives demonstrate the functionality of intracellular GPR30, *ACS Chem. Biol. 2*, 536–544.
6. Filardo, E., Quinn, J., Pang, Y., Graeber, C., Shaw, S., Dong, J., and Thomas, P. (2007) Activation of the novel estrogen receptor G protein-coupled receptor 30 (GPR30) at the plasma membrane, *Endocrinology 148*, 3236–3245.
7. Bologa, C. G., Revankar, C. M., Young, S. M., Edwards, B. S., Arterburn, J. B., Kiselyov, A. S., Parker, M. A., Tkachenko, S. E., Savchuck, N. P., Sklar, L. A., Oprea, T. I., and Prossnitz, E. R. (2006) Virtual and biomolecular screening converge on a selective agonist for GPR30, *Nat. Chem. Biol. 2*, 207–212.
8. Dennis, M. K., Burai, R., Ramesh, C., Petrie, W. K., Alcon, S. N., Nayak, T. K., Bologa, C. G., Leitao, A., Brailoiu, E., Deliu, E., Dun, N. J., Sklar, L. A., Hathaway, H. J., Arterburn, J. B., Oprea, T. I., and Prossnitz, E. R. (2009) In vivo effects of a GPR30 antagonist, *Nat. Chem. Biol. 5*, 421–427.
9. Blasko, E., Haskell, C. A., Leung, S., Gualtieri, G., Halks-Miller, M., Mahmoudi, M., Dennis, M. K., Prossnitz, E. R., Karpus, W. J., and Horuk, R. (2009) Beneficial role of the GPR30 agonist G-1 in an animal model of multiple sclerosis, *J. Neuroimmunol. 214*, 67–77.
10. Xu, H., Qin, S., Carrasco, G. A., Dai, Y., Filardo, E. J., Prossnitz, E. R., Battaglia, G., Doncarlos, L. L., and Muma, N. A. (2009) Extranuclear estrogen receptor GPR30 regulates serotonin function in rat hypothalamus, *Neuroscience 158*, 1599–1607.
11. Haas, E., Bhattacharya, I., Brailoiu, E., Damjanovic, M., Brailoiu, G. C., Gao, X., Mueller-Guerre, L., Marjon, N. A., Gut, A., Minotti, R., Meyer, M. R., Amann, K., Ammann, E., Perez-Dominguez, A., Genoni, M., Clegg, D. J., Dun, N. J., Resta, T. C., Prossnitz, E. R., and Barton, M. (2009) Regulatory role of G protein-coupled estrogen receptor for vascular function and obesity, *Circ. Res. 104*, 288–291.
12. Teng, J., Wang, Z. Y., Prossnitz, E. R., and Bjorling, D. E. (2008) The G protein-coupled receptor GPR30 inhibits human urothelial cell proliferation, *Endocrinology 149*, 4024–4034.
13. Olde, B., and Leeb-Lundberg, L. M. (2009) GPR30/GPER1: searching for a role in estrogen physiology, *Trends Endocrinol. Metab. 20*, 409–416.
14. Martensson, U. E., Salehi, S. A., Windahl, S., Gomez, M. F., Sward, K., Daszkiewicz-Nilsson, J., Wendt, A., Andersson, N., Hellstrand, P., Grande, P. O., Owman, C., Rosen, C. J., Adamo, M. L., Lundquist, I., Rorsman, P., Nilsson, B. O., Ohlsson, C., Olde, B., and Leeb-Lundberg, L. M. (2009) Deletion of the G protein-coupled receptor 30 impairs glucose tolerance, reduces bone growth, increases blood pressure, and eliminates estradiol-stimulated insulin release in female mice, *Endocrinology 150*, 687–698.
15. Filardo, E. J., Graeber, C. T., Quinn, J. A., Resnick, M. B., Giri, D., DeLellis, R. A., Steinhoff, M. M., and Sabo, E. (2006) Distribution of GPR30, a seven membrane-spanning estrogen receptor, in primary breast cancer and its association with clinicopathologic determinants of tumor progression, *Clin. Cancer Res. 12*, 6359–6366.
16. Smith, H. O., Leslie, K. K., Singh, M., Qualls, C. R., Revankar, C. M., Joste, N. E., and Prossnitz, E. R. (2007) GPR30: a novel indicator of poor survival for endometrial carcinoma, *Am. J. Obstet. Gynecol. 196*, e381–389; discussion e389−311.
17. Smith, H. O., Arias-Pulido, H., Kuo, D. Y., Howard, T., Qualls, C. R., Lee, S. J., Verschraegen, C. F., Hathaway, H. J., Joste, N. E., and Prossnitz, E. R. (2009) GPR30 predicts poor survival for ovarian cancer, *Gynecol. Oncol. 114*, 465–471.
18. Mortimer, J. E., Dehdashti, F., Siegel, B. A., Katzenellenbogen, J. A., Fracasso, P., and Welch, M. J. (1996) Positron emission tomography with 2-[18F]fluoro-2-deoxy-D-glucose and 16α-[18F]fluoro-17β-estradiol in breast cancer: correlation with estrogen receptor status and response to systemic therapy, *Clin. Cancer Res. 2*, 933–939.
19. Tsujikawa, T., Yoshida, Y., Mori, T., Kurokawa, T., Fujibayashi, Y., Kotsuji, F., and Okazawa, H. (2008) Uterine tumors: pathophysiologic imaging with 16α-[18F]fluoro-17β-estradiol and 18F fluorodeoxyglucose PET−initial experience, *Radiology 248*, 599–605.

20. Yoshida, Y., Kurokawa, T., Tsujikawa, T., Okazawa, H., and Kotsuji, F. (2009) Positron emission tomography in ovarian cancer: 18F-deoxy-glucose and 16α-18F-fluoro-17β-estradiol PET, *J. Ovarian Res. 2*, 7.
21. Yoshida, Y., Kurokawa, T., Sawamura, Y., Shinagawa, A., Okazawa, H., Fujibayashi, Y., and Kotsuji, F. (2007) The positron emission tomography with F18 17β-estradiol has the potential to benefit diagnosis and treatment of endometrial cancer, *Gynecol. Oncol. 104*, 764–766.
22. Linden, H. M., Stekhova, S. A., Link, J. M., Gralow, J. R., Livingston, R. B., Ellis, G. K., Petra, P. H., Peterson, L. M., Schubert, E. K., Dunnwald, L. K., Krohn, K. A., and Mankoff, D. A. (2006) Quantitative fluoroestradiol positron emission tomography imaging predicts response to endocrine treatment in breast cancer, *J. Clin. Oncol. 24*, 2793–2799.
23. Dehdashti, F., Mortimer, J. E., Trinkaus, K., Naughton, M. J., Ellis, M., Katzenellenbogen, J. A., Welch, M. J., and Siegel, B. A. (2009) PET-based estradiol challenge as a predictive biomarker of response to endocrine therapy in women with estrogen-receptor-positive breast cancer, *Breast Cancer Res. Treat. 113*, 509–517.
24. Ramesh, C., Nayak, T. K., Burai, R., Dennis, M. K., Hathaway, H. J., Sklar, L. A., Prossnitz, E. R., and Arterburn, J. B. (2010) Synthesis and characterization of iodinated tetrahydroquinolines targeting the G protein-coupled estrogen receptor GPR30, *J. Med. Chem. 53*, 1004–1014.
25. Lashley, M. R., Niedzinski, E. J., Rogers, J. M., Denison, M. S., and Nantz, M. H. (2002) Synthesis and estrogen receptor affinity of a 4-hydroxytamoxifen-labeled ligand for diagnostic imaging, *Bioorg. Med. Chem. 10*, 4075–4082.
26. Banerjee, S., Das, T., Chakraborty, S., Samuel, G., Korde, A., Venkatesh, M., and Pillai, M. R. (2005) An estradiol-conjugate for radiolabelling with 177Lu: an attempt to prepare a radiotherapeutic agent, *Bioorg. Med. Chem. 13*, 4315–4322.
27. Delpassand, E. S., Yang, D. J., Wallace, S., Cherif, A., Quadri, S. M., Price, J., Joubert, A., Inoue, T., and Podoloff, D. A. (1996) Synthesis, biodistribution, and estrogen receptor scintigraphy of indium-111-diethylenetriaminepentaacetic acid-tamoxifen analogue, *J. Pharm. Sci. 85*, 553–559.
28. Gunanathan, C., Pais, A., Furman-Haran, E., Seger, D., Eyal, E., Mukhopadhyay, S., Ben-David, Y., Leitus, G., Cohen, H., Vilan, A., Degani, H., and Milstein, D. (2007) Water-soluble contrast agents targeted at the estrogen receptor for molecular magnetic resonance imaging, *Bioconjugate Chem. 18*, 1361–1365.
29. Lewis, M. R., Raubitschek, A., and Shively, J. E. (1994) A facile, water-soluble method for modification of proteins with DOTA. Use of elevated temperature and optimized pH to achieve high specific activity and high chelate stability in radiolabeled immunoconjugates, *Bioconjugate Chem. 5*, 565–576.
30. Deshpande, S. V., DeNardo, S. J., Kukis, D. L., Moi, M. K., McCall, M. J., DeNardo, G. L., and Meares, C. F. (1990) Yttrium-90-labeled monoclonal antibody for therapy: labeling by a new macrocyclic bifunctional chelating agent, *J. Nucl. Med. 31*, 473–479.
31. Wu, S. L., Johnson, K. A., and Horrocks, W. D., Jr. (1997) Kinetics of formation of Ca(2+) complexes of acyclic and macrocyclic poly(amino carboxylate) ligands: bimolecular rate constants for the fully-deprotonated ligands reveal the effect of macrocyclic ligand constraints on the rate-determining conversions of rapidly-formed intermediates to the final complexes, *Inorg. Chem. 36*, 1884–1889.
32. Ramesh, C., Bryant, B., Nayak, T., Revankar, C. M., Anderson, T., Carlson, K. E., Katzenellenbogen, J. A., Sklar, L. A., Norenberg, J. P., Prossnitz, E. R., and Arterburn, J. B. (2006) Linkage effects on binding affinity and activation of GPR30 and estrogen receptors ERα/β with tridentate pyridin-2-yl hydrazine tricarbonyl-Re/(99m)Tc(I) chelates, *J. Am. Chem. Soc. 128*, 14476–14477.
33. Nayak, T. K., Hathaway, H. J., Ramesh, C., Arterburn, J. B., Dai, D., Sklar, L. A., Norenberg, J. P., and Prossnitz, E. R. (2008) Preclinical development of a neutral, estrogen receptor-targeted, tridentate 99mTc(I)-estradiol-pyridin-2-yl hydrazine derivative for imaging of breast and endometrial cancers, *J. Nucl. Med. 49*, 978–986.